physica status solidi a
www.pss-a.com

Evaluation of Material Systems for THz Quantum Cascade Laser Active Regions

Hermann Detz, Aaron M. Andrews, Martin A. Kainz, Sebastian Schönhuber, Tobias Zederbauer, Donald MacFarland, Michael Krall, Christoph Deutsch, Martin Brandstetter, Pavel Klang, Werner Schrenk, Karl Unterrainer, and Gottfried Strasser*

Quantum cascade lasers (QCLs) have been realized in several different material systems. In the mid-infrared, active regions are predominantly based on $In_{0.53}Ga_{0.47}As$ and InAs as quantum well material. Market-ready devices routinely provide continuous-wave operation at room temperature. For their THz counterparts, the situation is less clear. The most common material system for THz QCLs is the inherently lattice-matched combination of GaAs with $Al_{0.15}Ga_{0.85}As$ barriers. Yet, these devices still only reach a maximum operating temperature of 200 K with a lack of progress within the past years. Based on the identification of key parameters, this work reviews material systems for quantum cascade lasers with an emphasis on material and growth-related aspects and the goal to identify promising candidates for future device generations. Similar active regions realized in different material systems allow to estimate the gain per unit thickness, as well as total growth times and relative thickness errors.

1. Introduction

Shortly after the first MIR QCL was demonstrated using $In_{0.53}Ga_{0.47}As/In_{0.52}Al_{0.48}As$ superlattices, the concept was succesfully extended to other InP-, GaAs-, and InAs-based material combinations.[1–4] GaAs-based devices suffer from lower optical gain due to the higher effective mass (m^*) as well as from the lack of dielectric waveguiding with the substrate, which still prevents continuous-wave operation at room temperature.[5] Although InAs/$AlAs_{0.16}Sb_{0.84}$ heterostructures theoretically offer higher gain, they also manifest technological challenges regarding epitaxial growth and waveguiding.[6]

The selection of a particular material system for a MIR QCL is mainly driven by the target wavelength. The work horse for wavelengths between 3 and 24 µm are $In_xGa_{1-x}As/In_yAl_{1-y}As/InP$ heterostructures including strain-compensated variants.[7,8] The main reasons for the dominance of this material system over GaAs and InAs heterostructures are the higher optical gain and the inherent ability for vertical dielectric waveguiding as well as the technological maturity. Yet, there are limits to the achievable wavelength range, as shown in **Figure 1**. Shorter wavelengths require a higher CBO, which can be achieved using $In_{0.53}Ga_{0.47}As/AlAs_{0.56}Sb_{0.44}$ or InAs/$AlAs_{0.16}Sb_{0.84}$ heterostructures, for wavelengths as low as 2.6 µm.[9,10] On the long wavelength end of the MIR region, most QCL material systems hit their limit with the onset of the AlAs Reststrahlenband near 25 µm.[7,11] The longest MIR wavelength of InAs/$AlAs_{0.16}Sb_{0.84}$-based devices is currently around 20 µm.[12] The only material system that allows longer MIR emission wavelengths is the Al-free combination of $In_{0.53}Ga_{0.47}As$ with $GaAs_{0.51}Sb_{0.49}$ barriers, which avoids the Reststrahlenband absorption of AlAs phonons.[13]

For THz QCL active regions, the situation regarding the optimum material system is not yet so clear. The main hurdle is mainly the limited maximum operating temperature of presently 200 K. Until now, the best performing devices were exclusively based on GaAs/$Al_xGa_{1-x}As$ heterostructures, yet with an evident lack of progress within the past years.[15–17] Structural imperfections like interface roughness, compositional grading, or residual doping are known to play a role for MIR devices, but are not understood in full detail at this point.[18–20]

This article summarizes the choice of the material system on THz QCL active regions as well as growth-related effects that are interlinked. The main emphasis is developments in the active material of QCLs and therefore material-related advances

Dr. H. Detz, Dr. A. M. Andrews, Dr. T. Zederbauer, D. MacFarland, Dr. P. Klang, Dr. W. Schrenk, Prof. G. Strasser
Center for Micro- and Nanostructures and Institute of Solid-State Electronics
Nano – Center Campus Gußhaus
TU Wien
Gußhausstrasse 25–25a, 1040 Wien, Austria
E-mail: hermann.detz@tuwien.ac.at

Dr. H. Detz
Central European Institute of Technology
Brno University of Technology
Purkyňova 123, 612 00 Brno, Czech Republic

M. A. Kainz, S. Schönhuber, Dr. M. Krall, Dr. C. Deutsch, Dr. M. Brandstetter, Prof. K. Unterrainer
Photonics Institute
TU Wien
Gußhausstrasse 27, 1040 Wien, Austria

© 2018 The Authors. Published by WILEY-VCH Verlag GmbH & Co. KGaA, Weinheim. This is an open access article under the terms of the Creative Commons Attribution-NonCommercial License, which permits use, distribution and reproduction in any medium, provided the original work is properly cited and is not used for commercial purposes.

DOI: 10.1002/pssa.201800504

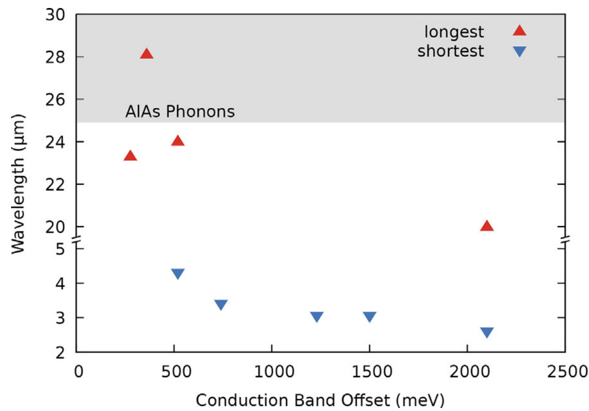

Figure 1. Shortest and longest MIR QCL wavelengths for different CBO.[14,7–13] Lasing within the AlAs Reststrahlenband is enabled by the Al-free combination of $In_{0.53}Ga_{0.47}As$ quantum wells and $GaAs_{0.51}Sb_{0.49}$ barriers.

in the waveguides like InP overgrowth for buried-heterostructure MIR QCL or alternative materials for double-metal THz QCL cavities are deliberately neglected.[21,22] Finally, the findings are compiled in a comparative analysis of the material systems, in which THz QCLs have already been demonstrated experimentally to identify promising candidates as well as critical parameters.

2. Growth Optimization

$GaAs/Al_xGa_{1\text{-}x}As$ heterostructures have reached a higher level of maturity than any other III–V material combination with respect to the epitaxial growth, processing technology, and material characterization. Despite this fact, seemingly insignificant details like the growth direction have been addressed only recently.[23] Improved GaAs-based THz QCL mainly rely on optimized models and layer sequences, which recently allowed to reach a T_{max} of 200 K.[24] In contrast to GaAs-based heterostructures, $In_{0.53}Ga_{0.47}As$ quantum wells with $In_{0.52}Al_{0.48}As$ or $GaAs_{0.51}Sb_{0.49}$ barriers – lattice-matched to InP – or InAs with $AlAs_{0.16}Sb_{0.84}$ or quaternary $Al_xIn_{1\text{-}x}As_{1\text{-}y}Sb_y$ barriers have not yet fully been optimized for the requirements of THz QCL active regions.

Many of the recent growth optimizations for low m^* $In_{0.53}Ga_{0.47}As$ and InAs-based THz QCL active regions, which are lined out in the following sections, were performed on nominally symmetric THz QCL active regions, grown by MBE.[25,26] Differences in the scattering rates between both bias polarities generally lead to asymmetric device characteristics, which can be assigned to particular growth-related issues.

2.1. Doping Level and Position

The carrier concentration within a QCL active region requires careful optimization, as it influences both threshold and maximum current density. While the optical output power of THz QCL was found to scale with the doping level, the impact on the T_{max} is not so trivial.[27–29] **Figure 2** compiles the obtained T_{max} versus sheet carrier densities of recent THz QCL in different material systems. GaAs-based devices show their best performance around 3×10^{10} cm^{-2}.[15,22,27] The optimum trade-off between optical gain and reduced lifetimes due to increased carrier concentrations is found to be around $2 \times 10^{10}\,cm^{-2}$ $-3 \times 10^{10}\,cm^{-2}$ for $In_{0.53}Ga_{0.47}As$-based active regions, yet the limited number of available data points still prevents a more exact fit.[23,29]

Studies on symmetric active regions revealed the importance of the position of the dopant atoms within the injector of QCL active regions.[26,36] The nominally rectangular doping profile is actually smeared out along the growth direction. In the case of electron transport along growth direction, this leads to increased ionized impurity scattering in the vicinity of the upper laser level and consequently a higher threshold current density. This effect can be compensated by offsetting the doping counter the growth direction. Threshold current density ratios (J^-_{th}/J^+_{th}) for different doping profiles and center positions are compiled in **Figure 3**. Symmetric device characteristics can be obtained for setback lengths of 3.6 nm for $GaAs/Al_{0.15}Ga_{0.85}As$ and 4.7 nm for $In_{0.53}Ga_{0.47}As/In_{0.52}Al_{0.48}As$. Although the substrate temperature during growth is 70–120 K cooler for $In_{0.53}Ga_{0.47}As$-based structures, the effect is comparably strong as both materials require a doping setback of approximately 10% of the active region period. This can probably be attributed to the higher growth rates used for $In_{0.53}Ga_{0.47}As$-based structures. Although dopant migration is also present in $In_{0.53}Ga_{0.47}As/GaAs_{0.51}Sb_{0.49}$ structures, these can not directly be compared as the ratio of threshold current densities is dominated by interface roughness scattering.[37]

2.2. Group-V Mixing

Both of the two technologically most advanced material systems – $GaAs/Al_xGa_{1\text{-}x}As$ and $In_{0.53}Ga_{0.47}As/In_{0.52}Al_{0.48}As$ – are

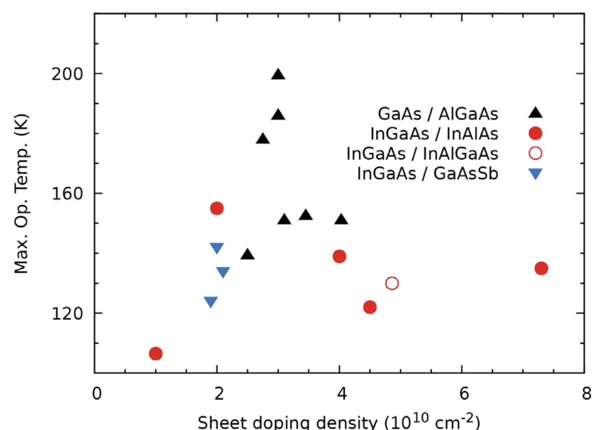

Figure 2. Maximum operating temperature of THz QCL around 3.8 THz for different sheet carrier concentrations and material systems.[15,16,22,23,29,30–35] The best performing GaAs –based devices were doped to approx. $3 \times 10^{10}\,cm^{-2}$. $In_{0.53}Ga_{0.47}As$-based QCLs perform best at similar sheet carrier concentrations around $2 \times 10^{10}\,cm^{-2}$ $-3 \times 10^{10}\,cm^{-2}$.

© 2018 The Authors. Published by WILEY-VCH Verlag GmbH & Co. KGaA, Weinheim

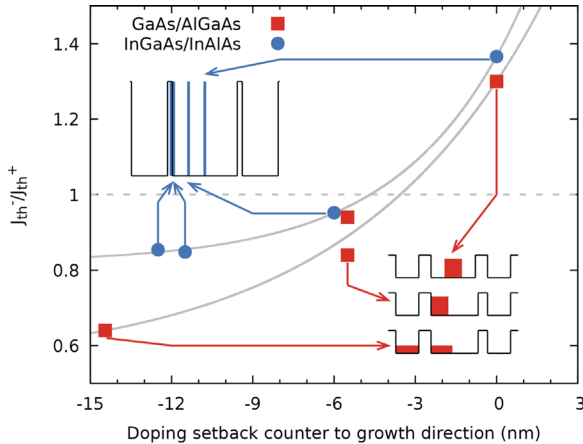

Figure 3. Threshold current density ratios (J^-_{th}/J^+_{th}) obtained for different doping positions in nominally symmetric THz QCL.[23] Dopant migration during MBE growth increases non-radiative scattering and therefore J_{th} for electron transport along growth direction. Symmetric device characteristics can be expected for doping offsets of 3.6 nm in GaAs and 4.7 nm in $In_{0.53}Ga_{0.47}As$. The data points correspond to the center positions of the doped regions, which are indicated in the insets.

composed of arsenide compounds only and therefore exhibit a continuous group V matrix. In contrast, low m^* material systems are generally based on alloys with mixed group V fractions. This applies to $InAs/AlAs_{0.16}Sb_{0.84}$ superlattices, where 16% of As are required within the barriers to maintain lattice-matching with the InAs substrate, but also to $In_{0.53}Ga_{0.47}As/GaAs_{0.51}Sb_{0.49}$ or quaternary barrier materials like $Al_xIn_{1-x}As_{1-y}Sb_y$.

In order to avoid building up strain within the active region, lattice-matching and consequently the group V composition must be controlled accurately. This is a delicate task, as the incorporation of group V species depends on several external parameters, like their flux ratios, the substrate temperature and growth rates. All of these have a direct impact on As-Sb exchange reactions, which have been observed for a range of materials.[38,39]

These reactions at the growth surface can be suppressed by lowering the substrate temperature below 430 °C.[40,41] For the growth of $GaAs_{1-x}Sb_x$, the crystal quality can furthermore be improved by using higher Ga fluxes, but at the cost of accuracy regarding the layer thicknesses, as discussed in section 4.

3. Design Considerations

The stagnation in the temperature performance of THz QCL requires a combined approach of careful optimizations regarding both, quantum-mechanical design as well as epitaxial growth. THz QCL will serve as illustrative example. Nevertheless, these arguments can be transferred to a wider range of heterostructures or functional devices.

3.1. Effective Mass Dependence of ISB Gain

The optical gain of ISB emitters is approximately proportional to $|z_{if}|^2\tau_i$, where z_{if} denotes the dipole matrix element for the optical transition and τ_i represents the lifetime in the initial state.[5] Realistic device models also need to take the population in the final state into account, which is neglected here for simplicity. The combination of these two components is proportional to $(m^*)^{-3/2}$. Therefore, low m^* materials provide higher optical gain per active period. Ref. [5] provides an experimental comparison of the EL intensity ratios for $GaAs/Al_xGa_{1-x}As$, $In_{0.53}Ga_{0.47}As/In_{0.52}Al_{0.48}As$ and $InAs/AlAs_{0.16}Sb_{0.84}$ ISB emitters.[42] In this work, the EL intensity of $In_{0.53}Ga_{0.47}As$-based active regions compared GaAs-based structures scales by a factor of 2.1, while InAs-based quantum wells surpass GaAs by a factor of 5.2. These data are close to the expected values based on the m^* ratios and are taken as an empirical measure to gauge the potential of different material systems for THz QCL.

At a given wavelength, different material parameters not only influence the optical gain per cascade, but also require modifications to the layer sequence to maintain the energy for the optical transition as well as the LO-phonon resonance.[23] In the case of low m^* materials, this generally leads to a larger active region period. A comparison of the values for the period and required lasing bias field for the three-well designs, which allow the highest T_{max} in each of the material systems, is shown in **Figure 4**.[15,29,23,43] It is worth noting that the product of period × lasing bias field remains almost constant, with deviations of less than 5% with respect to $GaAs/Al_xGa_{1-x}As$ between all material systems ($In_{0.53}Ga_{0.47}As/In_{0.52}Al_{0.48}As$: 2.2%, $In_{0.53}Ga_{0.47}As/GaAs_{0.51}Sb_{0.49}$: −3.4%, $InAs/AlAs_{0.16}Sb_{0.84}$: 1.3%), which demonstrates the similarity of the active region designs within this comparison.

This empirically determined relation between m^* and the period allows to relate experimentally obtained EL intensities with a unit thickness.[5] The corresponding values are plotted in **Figure 5**. Low m^* material systems are still favorable compared to GaAs from a theoretical perspective, yet the intensity ratio is

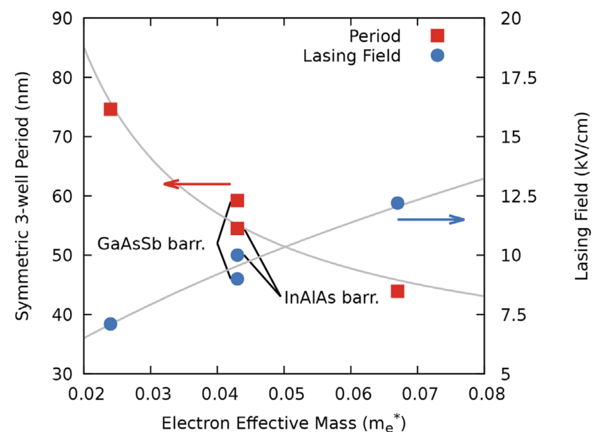

Figure 4. Active region period and required bias field for lasing operation versus. m^* for symmetric three-well THz QCL. The thickness of one active period increases by approx. 30% for $In_{0.53}Ga_{0.47}As$ and by 70% for InAs, both compared to GaAs. The bias field required for lasing operation shows the opposite relation and decreases by approx. 20% for $In_{0.53}Ga_{0.47}As$ and 40% for InAs.

© 2018 The Authors. Published by WILEY-VCH Verlag GmbH & Co. KGaA, Weinheim

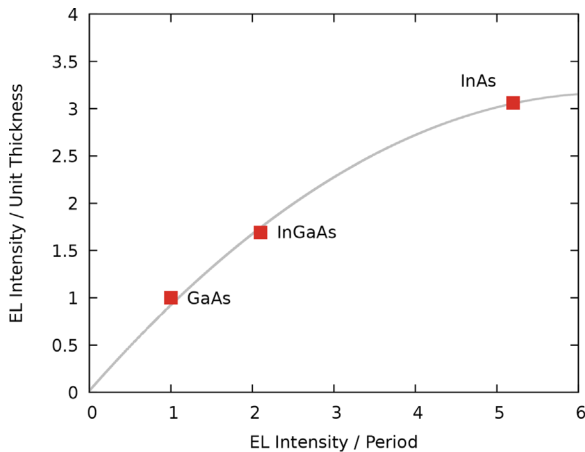

Figure 5. Relation between normalized intersubband EL intensity per period and per unit thickness. Experimental values were taken from ref. [5]. These data points were rescaled to a unit thickness using the active region period lengths of those three-well designs which currently provide the highest T_{max} for each material system. The solid line represents a guide for the eye.

reduced from 2.1 to 1.7 for $In_{0.53}Ga_{0.47}As$ and from 5.2 to 3.1 for InAs quantum wells.

3.2. Candiate Material Systems for THz QCLs

The above mentioned dependence of the ISB gain on the m^* can be used to estimate the potential of other material systems that being investigated, but where QCL operation has not been demonstrated yet. While the concept of intersubband emission could be extended to a wider range of materials, this evaluation is limited to materials, where electroluminescence has been demonstrated up to date.[44–49] Experimental EL data of established material systems are used to obtain a fit function with one free parameter.[5] The obtained relation $\mathrm{EL}(m^*) = 9.41 \times 10^{-4}(\pm 4 \times 10^{-5})m^{*-3/2}$ is then extrapolated towards other materials. Projected relative EL data of selected quantum well materials are plotted versus the respective carrier mass in **Figure 6**a.

It should also be noted that the m^* and therefore the expected optical gain of potential future THz QCL material systems is not the only parameter of interest. A larger m^* could possibly be compensated by a larger LO-phonon energy (E_{LO}). On the one hand, a higher E_{LO} provides a larger barrier for thermally activated relaxation, which needs to be overcome by the quantization and thermal distribution ($\hbar\omega + k_B T E_{LO}$).[50,51] On the other hand, a larger E_{LO} reduces thermal backfilling of the lower laser level, from the injector ground state of the next cascade.[52] Corresponding values are compiled in Figure 6b. It should be noted that the slightly higher E_{LO} is an advantage of GaAs compared to $In_{0.53}Ga_{0.47}As$ and InAs. In this respect, GaN or ZnO-based devices may still appear as interesting alternatives. A quantitative comparison of non-radiative scattering rates requires elaborate models, which are beyond the scope of this work.[53]

All of the higher E_{LO} candidate material systems share a challenging growth, which is not yet comparable to conventional III–V heterostructures. Crucial points are the lack of high-quality

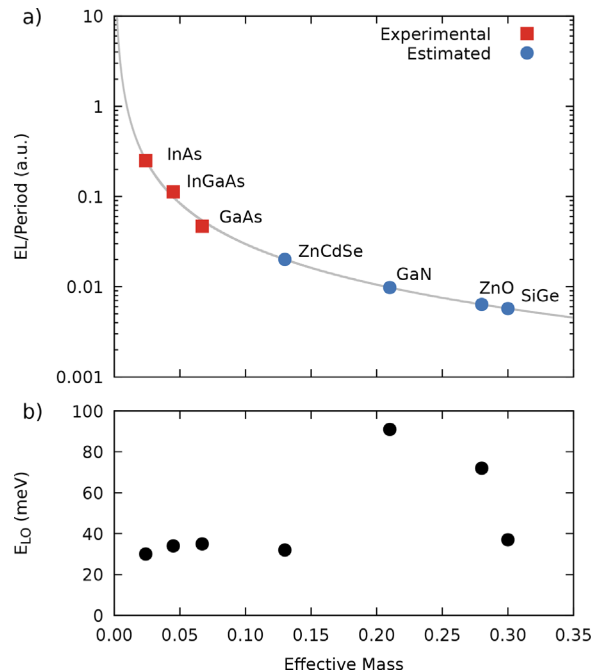

Figure 6. a) EL intensity per period versus m^*. Experimental data points are used to obtain a fit and estimate the potential of candidate material, in which QCL have not yet been demonstrated. With the exception of $Si_{1-x}Ge_x$, m^* refers to electrons. b) LO-phonon energies corresponding to the materials in (a). Due to their large E_{LO}, GaN or ZnO-based devices would be able to cover wavelengths within the Reststrahlenband of the other materials.

substrates for GaN or ZnO-based structures as well as inherent strain in $Si_{1-x}Ge_x$ or $GaN/Al_xGa_{1-x}N$ heterostructures, which limits the total thickness or requires metamorphic buffer layers. Furthermore, the active region design of GaN and ZnO-related materials is complicated due to their hexagonal crystal structure and resulting polarization charges. Therefore, the comparison of growth-related aspects in the following section focuses on material systems, where THz QCL have already been demonstrated.

4. Practical Aspects

Envelope function approximation based models of QCL active regions allow optimization of layer thicknesses and therefore quantum-mechanical wavefunctions at arbitrary precision. There are however some limitations which arise from material and growth-related aspects. The following paragraphs discuss practical considerations with an impact on heterostructure designs. Although the analysis is done for THz QCLs, these findings apply to other superlattices as well.

The underlying calculations were performed using the minimum required set of effusion cells in an MBE system for each material system. Therefore, the GR of $Al_xGa_{1-x}As$ at a given Al-content is not independent of the GaAs GR anymore. Conversely, only the combined growth rate of either $In_{0.53}Ga_{0.47}As$ or $In_{0.52}Al_{0.48}As$ can be chosen freely, while the other one is defined through the lattice-matching conditions,

© 2018 The Authors. Published by WILEY-VCH Verlag GmbH & Co. KGaA, Weinheim

when using a common In cell. This is a realistic assumption rather than a deliberate restriction as the calibration effort and deposition of source material onto closed shutters are minimized. Furthermore, the number of cell ports on MBE systems is limited and therefore often does not allow for fully doubled cell configurations.

The situation for the candidate material systems is slightly more complex due to several reasons: All of these combinations are inherently strained and therefore have a limited critical layer thickness that can be grown defect-free. Furthermore, GaN-based heterostructures are grown under Ga-rich growth conditions, which leads to a coupling between the Al and N flux rather than between group III elements as for other III–V combinations. Due to these reasons and the lack of operational heterostructure designs, combinations, where lasing has not yet been achieved, were excluded from a more detailed analysis.

4.1. Growth Rates and Time

Calculated combinations of GR using fixed GR of 1 μm h^{-1} for the quantum well material are compiled in **Figure 7**a. GaAs/$Al_{0.15}Ga_{0.85}As$ and $In_{0.53}Ga_{0.47}As/In_{0.52}Al_{0.48}As$ heterostructures lead to a GR of the barrier material that exceeds the GR of the well material. In the case of $In_{0.53}Ga_{0.47}As/GaAs_{0.51}Sb_{0.49}$, the barrier GR is approximately half that of the well material. The lack of common cations in $InAs/AlAs_{0.16}Sb_{0.84}$ allows an independent choice of both respective GR. The data point shown in 7a corresponds to the value used in experimental reports.[43] The fixed GR ratios directly influence the relative thickness errors, as discussed in section 4.2.

Typical $Si_{1-x}Ge_x$ multi-quantum well structures in which electroluminescence in the THz range has been demonstrated use Ge fractions in the range of 0.25–0.50 and therefore would lead to a critical layer thickness of 40 to 20 nm.[49,54] The combination of thicker $Si_{1-x}Ge_x$ quantum wells with thinner Si barriers would in general be favorable regarding thickness errors. Proposed GaN-based active regions with $Al_{0.15}Ga_{0.85}N$ barriers suffer from a similar critical layer thickness around 60 nm.[52,55,56] Such materials are therefore typically grown on relaxed metamorphic buffers to enable a higher number of active periods.

The differing GR ratios of the different material systems naturally have a direct impact on the total time that is required to grow a QCL active region. A total active region thickness of 10 μm has been established somewhat as a reference value, which translates into total growth times at the order of 10 h.[57] Calculated growth times, neglecting possible interruptions or differing GR for contact layers or etch-stop layers, are plotted in Figure 7b. The relatively high barrier GR of $Al_xGa_{1-x}As$ leads to relatively short total growth times for GaAs-based active regions, which are only marginally surpassed by the uncommon case of $In_{0.53}Ga_{0.47}As$ quantum wells with quaternary $In_{1-x-y}Al_xGa_yAs$ barriers. The case of $In_{0.53}Ga_{0.47}As/GaAs_{0.51}Sb_{0.49}$ stands out due to the fixed ratio of approximately 0.5 between barrier and well, which translates into a total growth time of 11.1 h. The InAs-based structures could in principle be grown faster due to the flexible barrier growth rate, although a trade-off between required time and resulting thickness errors needs to be considered. Scaling of these data for different growth rates is trivial and therefore left for the reader.

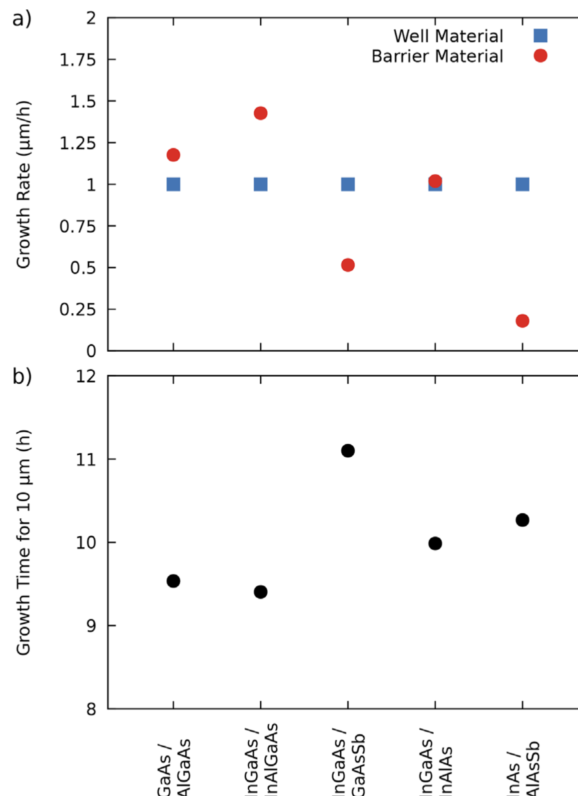

Figure 7. a) Calculated GR combinations for different material systems using a minimum set of effusion cells. The GR of the quantum well material was fixed at 1 μm h^{-1}. The GR for InAs and $AlAs_{0.16}Sb_{0.84}$ are independent of each other. The actual GR for $AlAs_{0.16}Sb_{0.84}$ was taken from ref. [43]. b) Resulting growth time for a THz QCL active region thickness of 10 μm, neglecting growth interruptions, etch-stop, and contact layers.

Although the process time represents a pure technological problem, long-term stability of cell temperature controls may affect the accuracy of the grown heterostructures. It should be noted that gradients due to possibly occurring cell depletion would correlate with the total thickness, but would be independent of the growth time.

4.2. Thickness Error Estimation

The material and growth-related considerations discussed so far can be combined to approach the material system selection for THz QCL from a practical perspective. The ability to tune the emission wavelength through a variation of the individual layer thicknesses is commonly considered as one of the major advantages of QCL. In order to maintain a spacing of quantized states on the energy axis that allows an optical transition in the THz range in combination with an LO-phonon resonance for depletion of the lower laser level and a comparable anticrossing energy for the different material systems, the contribution of the

© 2018 The Authors. Published by WILEY-VCH Verlag GmbH & Co. KGaA, Weinheim

barrier material to the superlattice period needs to be reduced with increasing CBO.[23] **Figure 8**a shows a barrier material fraction of 31% for GaAs/$Al_{0.15}Ga_{0.85}As$ and 2.7% for InAs/$AlAs_{0.16}Sb_{0.84}$. Correspondingly, the absolute layer thickness of the thinnest barrier needs to be scaled down. Minimum barrier thicknesses for the different material systems are summarized in Figure 8b. The floor was purposely set to 0.3 nm, which corresponds to a monolayer in the zincblende lattice. While models can easily deal with even thinner barriers, this was set as a reasonable minimum.[58]

The combination of design implications, like the dependence of the quantum well and barrier thicknesses on the m^*, with information on the growth process allows to calculate the relative thickness errors expected for quantum well and barrier layers in different material systems due to shutter operations. The error contributions due to deviations in the growth rate are neglected here, as they could in theory fully be compensated by proper calibration. Worst-case values, obtained for the thinnest well and barrier are plotted in Figure 8c. These were calculated based on the given thicknesses and growth rates under the assumption of a constant shutter reaction time of 150 ms, which is a typical value for MBE systems.

The fact that in all material systems, the total thickness of quantum well layers dominates over barriers leads to much smaller relative thickness errors since the reaction time of the cell shutters can be assumed to be independent of the chemical species. The higher combined growth rate of $In_{0.53}Ga_{0.47}As$, compared to GaAs or InAs causes the largest thickness errors of quantum wells due to shutter timing to be around 0.35%.

The same calculation, done for barrier layers results in relative thickness errors of up to 7.5%. Particularly, the combination of a high growth rate with a high CBO and therefore thin barrier layers in $In_{0.53}Ga_{0.47}As$/$In_{0.52}Al_{0.48}As$ stands out in this analysis. Although the $AlAs_{0.16}Sb_{0.84}$ barriers could be grown at an arbitrarily low growth rate, reasonable limitations due to total process time still lead to a thickness error of 2.5%, again caused by the high CBO. These examples underline the importance of a low barrier height to minimize thickness errors due to the finite time of shutter operations.

The need for ultra-thin barriers furthermore becomes relevant due to the required timing of shutter operations during MBE growth. A detailed discussion of the different cell and shutter geometries as well as of the different temperature control modes is beyond the scope of this work. Particularly the growth of QCL active regions requires a good compromise between long-term stability and the suppression of transients due to shutter operations. It is therefore desirable to minimize the shutter operations to allow a focus on flux stability. In this respect, the growth of GaAs/$Al_xGa_{1-x}As$ heterostructures is the simplest with only one shutter operation at each interface. Both $In_{0.53}Ga_{0.47}As$-based variations require two shutters to be opened or closed at each interface – Ga and Al in the case of $In_{0.52}Al_{0.48}As$ barriers or In and Sb in the case of $GaAs_{0.51}Sb_{0.49}$ barrier. Finally, InAs-based structures show the highest complexity due to the lack of a common cation and require three shutters to be operated at each interface. Although hard to quantify, this provides another argument for the GaAs dominance regarding THz QCL active regions.

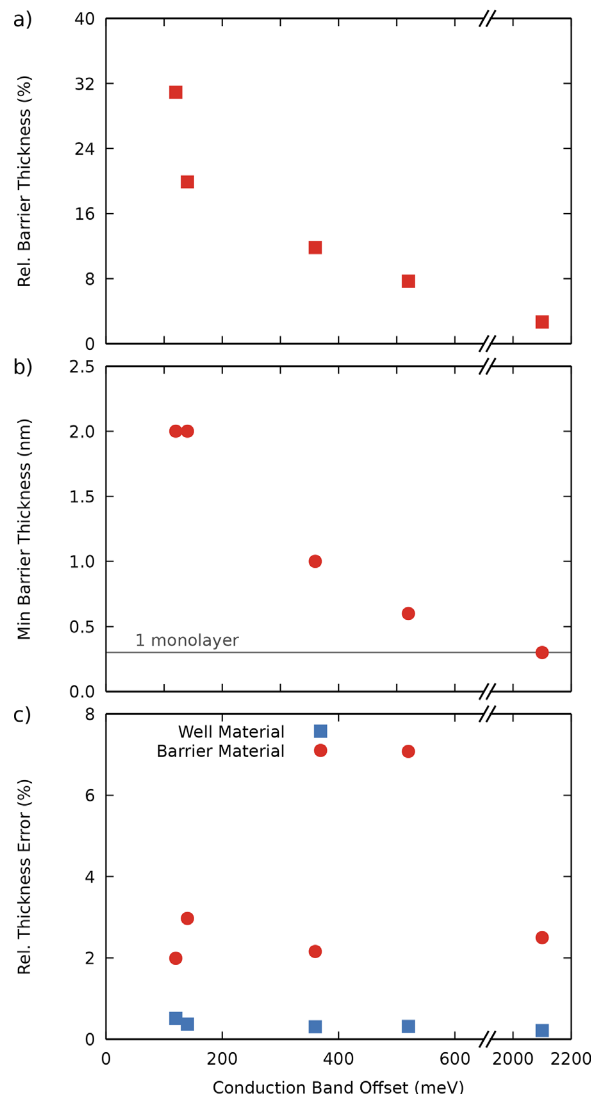

Figure 8. a) Relative barrier thickness in a THz QCL active region versus CBO that is, for different material systems. Data from refs. [15,29,23,35,43]. Higher CBO clearly lead to a diminishing fraction of barrier material. b) Mininum barrier thickness required to maintain an optical transition around 3.7 THz and the corresponding LO-phonon resonance for depletion of the lower laser level. The heterostructures were modeled with a fixed floor of 0.3 nm, approximately corresponding to one monolayer. c) Calculated relative thickness errors based on the minimum well and barrier thicknesses as well as on the growth rate combinations given in **Figure 7**. The thickness errors are caused by a finite reaction time of the MBE cell shutters. The lowest error for barriers is reached for $Al_xGa_{1-x}As$ at a CBO of 120 meV, due to the relatively large layer thickness. The combination of a relatively high CBO of 520 meV with a required fixed ratio of the $In_{0.53}Ga_{0.47}As$ and $In_{0.52}Al_{0.48}As$ growth rates causes the largest errors of just above 7%. Active regions with quaternary barriers, with a CBO of 140 meV, also show pronounced errors in the barrier thickness due to the relatively large fixed growth rate of $In_{1-x-y}Al_xGa_yAs$.

5. Conclusion

This article summarizes the present state-of-the-art. Novel candidate material systems for THz QCL are not only facing

© 2018 The Authors. Published by WILEY-VCH Verlag GmbH & Co. KGaA, Weinheim

technological challenges, but also inherent limitations, as the optical gain estimations in section 3.2 suggest. Nevertheless, these materials feature interesting aspects like e.g. the suppression LO-phonon scattering due to their large energy in GaN or the compatibility with conventional electronic platforms in the case of $Si_{1-x}Ge_x$.

While implications due to the choice of materials on growth rates and the total required time appear uncorrelated to the device performance at first sight, the long-term stability of effusion cells still causes a direct impact on the quality of grown active regions. With GaAs-based structures performing best, the current situation suggests that variations in the layer thickness, which are more pronounced for $In_{0.53}Ga_{0.47}As$-based material systems are more detrimental than the eventual long-term drift of effusion cells.

Acknowledgements

The authors acknowledge financial support by the Austrian Science Fund (FWF): H2N (P26100-N27), SFB NextLite (F49), and DK Solids4fun (WK1243) and by the Austrian Research Promotion Agency (FFG): COMTERA (849614). This work was partly supported by the ESF under the project CZ.02.2.69/0.0/0.0/16_027/0008371 and by AFOSR through the grant FA9550-17-1-0350. H.D. received funding through an APART Fellowship of the Austrian Academy of Sciences.

Conflict of Interest

The authors declare no conflict of interest.

Keywords

III–V heterostructures, intersubband devices, molecular beam epitaxy, quantum cascade lasers, superlattices

Received: June 30, 2018
Revised: August 22, 2018
Published online:

[1] J. Faist, F. Capasso, D. L. Sivco, C. Sirtori, A. L. Hutchinson, A. Y. Cho, *Science* **1994**, *264*, 553.
[2] C. Sirtori, P. Kruck, S. Barbieri, P. Collot, J. Nagle, M. Beck, J. Faist, U. Oesterle, *Appl. Phys. Lett.* **1998**, *73*, 3486.
[3] D. G. Revin, L. R. Wilson, E. A. Zibik, R. P. Green, J. W. Cockburn, M. J. Steer, R. J. Airey, M. Hopkinson, *Appl. Phys. Lett.* **2004**, *85*, 3992.
[4] J. Devenson, O. Cathabard, R. Teissier, A. N. Baranov, *Appl. Phys. Lett.* **2007**, *91*, 251102.
[5] E. Benveniste, A. Vasanelli, A. Delteil, J. Devenson, R. Teissier, A. Baranov, A. M. Andrews, G. Strasser, I. Sagnes, C. Sirtori, *Appl. Phys. Lett.* **2008**, *93*, 131108.
[6] A. N. Baranov, R. Teissier, *IEEE J. Sel. Top. Quantum Electron.* **2015**, *21*, 1200612.
[7] R. Colombelli, F. Capasso, C. Gmachl, A. L. Hutchinson, D. L. Sivco, A. Tredicucci, M. C. Wanke, A. M. Sergent, A. Y. Cho, *Appl. Phys. Lett.* **2001**, *78*, 2620.
[8] M. P. Semtsiv, M. Wienold, S. Dressler, W. T. Masselink, *Appl. Phys. Lett.* **2007**, *90*, 051114.
[9] D. G. Revin, J. P. Commin, S. Y. Zhang, A. B. Krysa, K. Kennedy, J. W. Cockburn, *IEEE J. Sel. Top. Quantum Electron.* **2011**, *17*, 1417.
[10] O. Cathabard, R. Teissier, J. Devenson, J. C. Moreno, A. N. Baranov, *Appl. Phys. Lett.* **2010**, *96*, 151110.
[11] J. Ulrich, J. Kreuter, W. Schrenk, G. Strasser, K. Unterrainer, *Appl. Phys. Lett.* **2002**, *80*, 3691.
[12] M. Bahriz, G. Lollia, A. N. Baranov, R. Teissier, *Opt. Express* **2015**, *23*, 1523.
[13] K. Ohtani, M. Beck, M. J. Süess, J. Faist, A. M. Andrews, T. Zederbauer, H. Detz, W. Schrenk, G. Strasser, *ACS Photonics* **2016**, *3*, 2280.
[14] J. Faist, F. Capasso, D. L. Sivco, A. L. Hutchinson, S. N. G. Chu, A. Y. Cho, *Appl. Phys. Lett.* **1998**, *72*, 680.
[15] S. Fathololoumi, E. Dupont, C. W. I. Chan, Z. R. Wasilewski, S. R. Laframboise, D. Ban, A. Mátyás, C. Jirauschek, Q. Hu, H. C. Liu, *Opt. Express* **2012**, *20*, 3866.
[16] Y. Chassagneux, Q. J. Wang, S. P. Khanna, E. Strupiechonski, J.-R. Coudevylle, E. H. Linfield, A. G. Davies, F. Capasso, M. A. Belkin, R. Colombelli, *IEEE Trans. Terahertz Sci. Technol.* **2012**, *2*, 83.
[17] S. Khanal, L. Zhao, J. L. Reno, S. Kumar, *J. Opt.* **2014**, *16*, 094001.
[18] Y. T. Chiu, Y. Dikmelik, P. Q. Liu, N. L. Aung, J. B. Khurgin, C. F. Gmachl, *Appl. Phys. Lett.* **2012**, *101*, 171117.
[19] C. Ndebeka-Bandou, F. Carosella, R. Ferreira, G. Bastard, *Appl. Phys. Lett.* **2013**, *102*, 191105.
[20] C. A. Wang, B. Schwarz, D. F. Siriani, L. J. Missaggia, M. K. Connors, T. S. Mansuripur, D. R. Calawa, D. McNulty, M. Nickerson, J. P. Donnelly, K. Creedon, F. Capasso, *IEEE J. Sel. Top. Quantum Electron.* **2017**, *23*, 1200413.
[21] M. Beck, J. Faist, U. Oesterle, M. Ilegems, E. Gini, H. Melchior, *IEEE Photon. Technol. Lett.* **2000**, *12*, 1450.
[22] M. A. Belkin, J. A. Fan, S. Hormoz, F. Capasso, S. P. Khanna, M. Lachab, A. G. Davies, E. H. Linfield, *Opt. Express* **2008**, *16*, 3242.
[23] C. Deutsch, M. Krall, M. Brandstetter, H. Detz, A. M. Andrews, P. Klang, W. Schrenk, G. Strasser, K. Unterrainer, *Appl. Phys. Lett.* **2012**, *101*, 211117.
[24] S. Fathololoumi, E. Dupont, Z. R. Wasilewski, C. W. I. Chan, S. G. Razavipour, S. R. Laframboise, S. Huang, Q. Hu, D. Ban, H. C. Liu, *J. Appl. Phys.* **2013**, *113*, 113109.
[25] C. Deutsch, H. Detz, T. Zederbauer, A. M. Andrews, P. Klang, T. Kubis, G. Klimeck, M. E. Schuster, W. Schrenk, G. Strasser, K. Unterrainer, *Opt. Express* **2013**, *21*, 7209.
[26] C. Deutsch, H. Detz, M. Krall, M. Brandstetter, T. Zederbauer, A. M. Andrews, W. Schrenk, G. Strasser, K. Unterrainer, *Appl. Phys. Lett.* **2013**, *102*, 201102.
[27] H. C. Liu, M. Wächter, D. Ban, Z. R. Wasilewski, M. Buchanan, G. C. Aers, J. C. Cao, S. L. Feng, B. S. Williams, Q. Hu, *Appl. Phys. Lett.* **2005**, *87*, 141102.
[28] A. Benz, G. Fasching, A. M. Andrews, M. Martl, K. Unterrainer, T. Roch, W. Schrenk, S. Golka, G. Strasser, *Appl. Phys. Lett.* **2007**, *90*, 101107.
[29] C. Deutsch, M. A. Kainz, M. Krall, M. Brandstetter, D. Bachmann, S. Schönhuber, H. Detz, T. Zederbauer, D. MacFarland, A. M. Andrews, W. Schrenk, M. Beck, J. Faist, G. Strasser, K. Unterrainer, *ACS Photonics* **2017**, *4*, 957.
[30] S. Kumar, Q. Hu, J. L. Reno, *Appl. Phys. Lett.* **2009**, *94*, 131105.
[31] S. Kumar, C. W. I. Chan, Q. Hu, J. L. Reno, *Nat. Phys.* **2010**, *7*, 166.
[32] M. Brandstetter, C. Deutsch, M. Krall, H. Detz, D. C. Mac-Farland, T. Zederbauer, A. M. Andrews, W. Schrenk, G. Strasser, K. Unterrainer, *Appl. Phys. Lett.* **2013**, *103*, 171113.
[33] S. G. Razavipour, E. Dupont, S. Fathololoumi, C. W. I. Chan, M. Linkdskog, Z. R. Wasilewski, G. Aers, S. R. Laframboise, A. Wacker, Q. Hu, D. Ban, H. C. Liu, *J. Appl. Phys.* **2013**, *113*, 203107.
[34] M. Fischer, G. Scalari, K. Celebi, M. Amanti, Ch. Walther, M. Beck, J. Faist, *Appl. Phys. Lett.* **2010**, *97*, 221114.

© 2018 The Authors. Published by WILEY-VCH Verlag GmbH & Co. KGaA, Weinheim

[35] K. Ohtani, M. Beck, G. Scalari, J. Faist, *Appl. Phys. Lett.* **2013**, *103*, 041103.
[36] P. M. Bouzi, Y. T. Chiu, C. Deutsch, Y. Dikmelik, Y. Song, V. Tokranov, S. Oktyabrsky, C. Gmachl, *J. Appl. Phys.* **2014**, *116*, 034504.
[37] C. Deutsch, H. Detz, T. Zederbauer, M. Krall, M. Brandstetter, A. M. Andrews, P. Klang, W. Schrenk, G. Strasser, K. Unterrainer, *J. Infrared Milli. Terahz. Waves* **2013**, *34*, 374.
[38] E. Selvig, B. O. Fimland, T. Skauli, R. Haakenaasen, *J. Crystal Growth* **2001**, *227-228*, 562.
[39] M. Losurdo, P. Capezzuto, G. Bruno, A. S. Brown, T. Brown, G. May, *J. Appl. Phys.* **2006**, *100*, 013531.
[40] T. Zederbauer, A. M. Andrews, D. MacFarland, H. Detz, W. Schrenk, G. Strasser, *Photonics* **2016**, *3*, 20.
[41] T. Zederbauer, A. M. Andrews, D. MacFarland, H. Detz, W. Schrenk, G. Strasser, *APL Mater.* **2017**, *5*, 035501.
[42] Benveniste et al. refer to the later material system as InAs/AlSb [5]. Inherent strain would prevent good growth quality. Lattice-matching is likely achieved through the incorporation of residual As.
[43] M. Brandstetter, M. A. Kainz, T. Zederbauer, M. Krall, S. Schönhuber, H. Detz, W. Schrenk, A. M. Andrews, G. Strasser, K. Unterrainer, *Appl. Phys. Lett.* **2016**, *108*, 011109.
[44] Y. Yao, A. Alfaro-Martinez, K. J. Franz, W. O. Charles, A. Shen, M. C. Tamargo, C. F. Gmachl, *Appl. Phys. Lett.* **2011**, *99*, 041113.
[45] L. Nevou, F. H. Julien, R. Colombelli, F. Guillot, E. Monroy, *Electron. Lett.* **2006**, *42*, 1308.
[46] D. Hofstetter, D. P. Bour, L. Kirste, *Appl. Phys. Lett.* **2014**, *104*, 241107.
[47] A. Y. Song, R. Bhat, A. A. Allerman, J. Wang, T.-Y. Huang, C.-E. Zah, C. F. Gmachl, *Appl. Phys. Lett.* **2015**, *107*, 132104.
[48] G. Dehlinger, L. Diehl, U. Gennser, H. Sigg, J. Faist, K. Ensslin, D. Grützmacher, E. Müller, *Science* **2000**, *290*, 2277.
[49] S. A. Lynch, R. Bates, D. J. Paul, D. J. Norris, A. G. Cullis, Z. Ikonic, R. W. Kelsall, P. Harrison, D. D. Arnone, C. R. Pidgeon, *Appl. Phys. Lett.* **2002**, *81*, 1543.
[50] T.-T. Lin, K. Ohtani, H. Ohno, *Appl. Phys. Express* **2009**, *2*, 022102.
[51] J. Faist, *Quantum Cascade Lasers*. Oxford University Press, Oxford **2013**.
[52] G. Sun, R. A. Soref, J. B. Khurgin, *Superlattices Microstruct.* **2005**, *37*, 107.
[53] C. Jirauschek, T. Kubis, *Appl. Phys. Rev.* **2014**, *1*, 011307.
[54] G. Matmon, D. J. Paul, L. Lever, M. Califano, Z. Ikonić, R. W. Kelsall, J. Zhang, D. Chrastina, G. Isella, H. von Känel, E. Müller, A. Neels, *J. Appl. Phys.* **2010**, *107*, 053109.
[55] E. Bellotti, K. Driscoll, T. D. Moustakas, R. Paiella, *Appl. Phys. Lett.* **2008**, *92*, 101112.
[56] K. Wang, T. Grange, T.-T. Lin, L. Wang, Z. Jén, S. Birner, J. Yun, W. Terashima, H. Hirayama, *Appl. Phys. Lett.* **2018**, *113*, 061109.
[57] B. Williams, *Nat. Photon.* **2007**, *1*, 517.
[58] The authors are aware that growth programs would in principle allow arbitrarily thin layers, yet thicknesses below 0.3 nm do not lead to closed layers and are furthermore subject to shutter timing limitations and variations.

© 2018 The Authors. Published by WILEY-VCH Verlag GmbH & Co. KGaA, Weinheim